Journal of Power Sources 294 (2015) 284–291

Contents lists available at ScienceDirect

Journal of Power Sources

journal homepage: www.elsevier.com/locate/jpowsour

Thermal decomposition of alkane hydrocarbons inside a porous Ni anode for fuel supply of direct carbon fuel cell: Effects of morphology and crystallinity of carbon

Chengguo Li, Hakgyu Yi, Tahereh Jalalabadi, Donggeun Lee*

School of Mechanical Engineering, Pusan National University, Busan 609-735, South Korea

HIGHLIGHTS

- A first practical method to maximize triple phase boundary at DCFC fuel electrode.
- Carbon spheres, nanotubes, and nanofibers are produced under control.
- Less crystalline nanotubes and nanofibers are more active for longer time period.
- Power density and lifetime are even comparable to H_2-fuel fuel cell.

ARTICLE INFO

Article history:
Received 31 December 2014
Received in revised form
12 March 2015
Accepted 14 June 2015
Available online xxx

Keywords:
Direct carbon fuel cell (DCFC)
Carbon fueling
Porous anode
Hydrocarbon decomposition
Triple phase boundary

ABSTRACT

This study improved the physical contact between anode and fuel in a direct carbon fuel cell (DCFC) by directly generating carbon in a porous Ni anode through thermal decomposition of three kinds of hydrocarbons (CH_4, C_2H_6, C_3H_8). From electron microscope observations of the carbon particles generated from each hydrocarbon, carbon spheres (CS), carbon nanotubes (CNT) and carbon nanofibers (CNF) were identified with increasing carbon number. Raman scattering analysis was performed to determine the crystallinity of the carbon samples. As a result, the carbon samples (CS, CNT, and CNF) produced from CH_4, C_2H_6 and C_3H_8 were found to be less crystalline and more flexible with increasing the carbon number. DCFC performance was measured at 700 °C for the anode fueled with the same mass of the carbon sample. It was found that the 1-dimensional CNT and CNF were more active to produce 148% and 210% times higher power density than the CS. The difference was partly attributed to the finding that the less-crystalline CNT and CNF had much lower charge transfer resistances than the CS. A lifetime test found that the CNT and CNF, which are capable of transporting electrons for much longer periods, maintained the power density much longer, as compared to the CS which can lose their point contacts between the particles shortly at high current density.

1. Introduction

A direct carbon fuel cell (DCFC) does not require CO_2 separation as it only releases CO_2 [1,2]; such a cell also offers advantages in terms of fuel diversity and efficiency due to its ability to use various carbon solids as fuel [1–7]. DCFCs have thus gained the interest of researchers and users around the world. However, unlike gaseous fuel, which is known for being highly diffusible, solid fuels have essentially very limited contacts with anode and electrolyte. This would be a possible reason why the power density of DCFCs tends to be far lower than that of hydrogen-used fuel cells. Moreover, long-term operation with continuous or at least piecewise continuous refueling has not been achieved, and research is being actively conducted on the basis of button cells. Instead of utilizing the advantages of solid fuel, researchers have begun to work on modifying solid fuel to CO through various gasification methods such as the reverse Boudouard reaction ($C + CO_2 = 2CO$) [8–12], a catalytic reaction of C with molten carbonate [13,14] or hydrocarbon decomposition [15–19]. Since such approaches lead to simply other versions of gas-fueled molten carbonate fuel cells (MCFC) or solid oxide fuel cells (SOFC), we have turned our attention back to developing a practical way to solve the technical challenges of

* Corresponding author.
E-mail address: donglee@pusan.ac.kr (D. Lee).

http://dx.doi.org/10.1016/j.jpowsour.2015.06.079
0378-7753/

DCFCs: the limited triple phase boundary (TPB) and discontinuous refueling.

As for the issue of limited TPB, there have been a few previous reports proposing new ideas to overcome this problem. For example, some researchers [11,15,20] mixed carbon powder for a fuel, Ni or NiO powder for an anode, and YSZ or SDC powder for a solid electrolyte, and formed a plate-type C-fueled anode in attempts to increase the TPB. Despite the enhanced TPB and high working temperatures (700–900 °C), which might accelerate the electrochemical reaction kinetics, the power density was still less than 110 mW/cm^2. More recently, we made an attempt to increase the TPB by filling the inside of a porous Ni anode with carbon powders and coating the anode with a ceria to enhance the wettability. As a result, the power density of the new button cell was increased by a factor of 7 as compared to the case of a flat interface between fuel and electrode [21]. It should be noted that the dramatic increase of the performance was obtained even below 700 °C, at which temperatures the reverse Boudouard reaction is thermodynamically minimized. Thus we believe that the promising result was mainly attributable to the enhanced TPB.

As for the issue of discontinuous refueling, which limits long-term operation of DCFC, Lim et al. [9] succeeded in running DCFC for 200 h using CO generated from the reverse Boudouard reaction at 750 °C. However, it is noted that fuel reforming from the Boudouard reaction is only possible at temperatures higher than 700 °C. In addition to the problem of fuel supply, extensive research is being conducted on lowering the operating temperature of SO- or MC-based DCFCs [22]. In summary, there is no practical method that will support the expansion of TPB at lower temperatures and the continuous refueling as well. Among various methods, hydrocarbon decomposition comes close to meeting the aforementioned requirements.

Thermal decomposition or catalytic decomposition of hydrocarbon, together with the typical steam reforming process, has been widely studied to create syngas of H_2 & CO [23,24]. On the other hand, there have been a few interesting attempts to utilize methane gas as a carbon source for DCFCs through the decomposition of the gas in the absence of any oxygen source. For example, Li et al. [19] produced carbon nanofiber (CNF) through thermal decomposition of CH_4 at 500–700 °C for 35–75 h. The CNF fuels were then floated in a pool of molten carbonate in which a rod-shaped Au anode was installed. The power density, when measured at 800 °C, was 45 mW/cm^2 even for an unrealistically long fueling time. Ihara et al. supplied methane (CH_4) [16,17] and propane (C_3H_8) [18] to a Ni-GDC (gadolinium-doped ceria) porous cermet anode maintaining at 900 °C, to stimulate thermal decomposition. Gaseous residuals such as CH_4 and H_2, generated from the 5–360 min of thermal decomposition, were removed with carrier gas (argon), and only solid carbon formed between the building components of the anode was used as a fuel. A maximum power density of 80 mW/cm^2 was achieved as a result. Likewise, Li et al. [15] inserted methane (CH_4) gas into a Ni-YSZ cermet anode, maintained at 800 °C, to produce carbon in pores between anode particles. Next, SO-DCFC was activated based on carbon alone after removing gaseous products from the methane decomposition. A maximum power density was again 80 mW/cm^2. It is noted that the solid fuel tends to be unstable as the reverse Boudouard reaction is dominant at their operating temperature of 800–900 °C, resulting in low fuel utilization. Thus, the operating time ended up shortly; power density decreased 50% within 20 min.

In the present study, we directly produced carbon in a porous Ni anode through thermal decomposition of three different hydrocarbons (CH_4, C_2H_6, C_3H_8) at lower temperatures for 30 min, in an attempt to improve physical contact between the electrode and fuel. The carbon particles, generated from each hydrocarbon, were characterized in terms of the morphology and crystallinity using electron microscope and Raman spectroscopy. An MC-DCFC system was developed for the three different anodes fueled with the same mass of carbon; the performance was assessed at 700 °C. Longer chains of hydrocarbon are preferred for reducing the decomposition temperatures and producing more active carbon fuels. Possible cause will be discussed.

2. Experimental section

2.1. Sample preparation

Fig. 1 shows an experimental setup used for carbon formation in a porous Ni anode through hydrocarbon decomposition. A 6 cm-long 1.8 cm-thick cylindrical porous Ni foam (with a pore size of 50–75 μm) to be used as an anode was installed inside a quartz tube (80 cm × 1.85 cm). The quartz tube was placed in the middle of a hot-wall tube furnace (w/30 cm-long hot zone) and heated constantly at a certain temperature in a range of 500–900 °C. Methane (CH_4), ethane (C_2H_6) and propane (C_3H_8), with different carbon numbers among alkane hydrocarbons, were chosen as a carbon precursor. A gaseous hydrocarbon among them flowed alone through the hot porous Ni foam, at a rate of 55 ml/min, leading to carbon formation in between metal networks of the Ni foam. Thus, we believe that the carbon fuel makes good physical contact with Ni network. The amount of carbon formed was quite easy to control, simply by varying the furnace temperature or time period of hydrocarbon decomposition. Each hydrocarbon flow lasted constantly for 30 min, unless otherwise noted.

The Ni foam containing carbon samples generated from the hydrocarbons was cut into slices and the carbon morphology in the slice was investigated with a scanning electron microscopy (SEM; S-4800, Hitachi, 10 kV). The carbon particles were brushed from the Ni foam and then dispersed in ethanol with an ultrasonicator. A few drops of the carbon–ethanol suspension were dropped onto a TEM grid by using a micropipette, and then dried at room temperature. Detail microstructure of the carbon particles were observed with a high-resolution transmission electron microscopy (HRTEM; JEOL 2100F, 200 kV). In addition, the crystallinity of the carbon particles was analyzed by Raman spectroscopy (inVia Raman microscope, Renishaw) using a 514 nm Ar laser light, and X-ray diffraction (XRD, D/max 2400, Rigaku). More details of characterization experiments are available elsewhere [25,26].

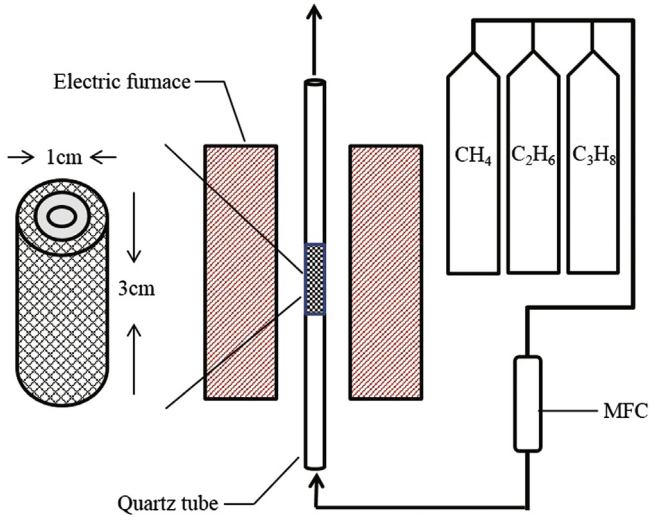

Fig. 1. A schematic diagram for carbon formation in a porous Ni anode through hydrocarbon decomposition.

2.2. DCFC system

Electrochemical oxidation characteristics of the carbon formed inside the porous Ni anode were measured in a three-electrode electrochemical cell, as shown in Fig. 2. The carbon (C)-containing cylindrical Ni anode was used as a working electrode (WE), after being spot-welded to a flat plate-type silver current collector (6 cm-high × 0.4 cm-thick). The counter electrode (CE) and reference electrode (RE) were made from a silver sheet (with 3.2 cm^2 surface area) spot-welded to a silver wire; the silver parts were each sheathed in a 12 mm diameter closed-bottom alumina tube. A 1.0 mm hole at the bottom of the alumina sheath allowed contact through the liquid electrolyte between the CE, RE and WE. For the electrolyte, after mixing Li_2CO_3 and K_2CO_3 in a mole ratio of 62:38, 350 g of the mixture was placed in an alumina container and melted at 700 °C. Thus, the C-containing WE was wetted in contact with the molten carbonate, resulting in a significant enhancement of the triple phase boundaries. It should be noted that the outer surface area (33.9 cm^2) of the cylindrical anode was used as a reference area for estimating the power and current density.

To remove residual oxygen in the system before carrying out the experiment, 50 ml/min of carbon dioxide was supplied to the CE and the RE, while heating the system to reach the operating temperature of 700 °C. When the operating temperature was attained, CO_2 and O_2 were mixed in a mole ratio of 2:1, and supplied to the CE and the RE at a flow rate of 99 ml/min. During the experiment, argon gas was supplied at 200 ml/min to the WE to purge the system of residual oxygen and CO_2. The I–V characteristics of the DCFC system were measured using an SP-150 Potentiostat/Galvanostat analyzer (Neoscience, Korea) with a scan rate of 1 mV/s. The electrical potential (V) as measured using the equipment indicates the voltage difference between the WE and the RE while the current is monitored from the WE to the CE. The power density was obtained simply by multiplying the current density (e. g. the current divided by outer surface area of the cylindrical anode) by the electrical potential at the current density. In order to figure the I–V characteristics out further, an electrochemical impedance spectroscopy (EIS) was measured with a SP-150 analyzer over the frequency between 0.6 Hz and 80 kHz.

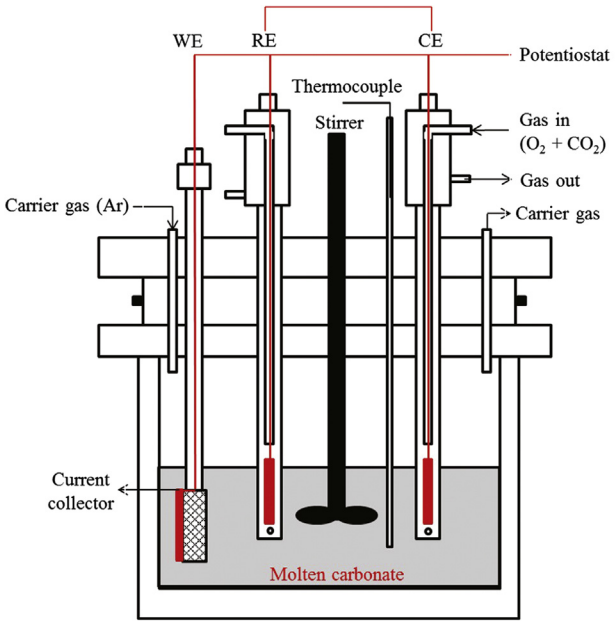

Fig. 2. A schematic diagram of the three-electrode DCFC system.

3. Results and discussion

Fig. 3 shows the relative amount of carbon ($\Delta m/m_0$) produced from thermal decomposition of the three hydrocarbons as a function of temperature; Δm denotes the mass increase of the Ni anode during the 30-min decomposition experiment and m_0 is an initial mass of the anode. The bar in Fig. 3 represents standard deviation of the relative carbon mass from three repeated experiments. As a result, CH_4 begins to decompose to produce carbon at 700 °C and the carbon production is noticeably accelerated at temperatures above 800 °C. Higher carbon number hydrocarbons turn out to produce carbon at lower temperatures. For example, 20% of carbon is produced from C_3H_8 at ~550 °C, far lower than 900 °C for CH_4. This result seems consistent with a previous report [27] in which alkane hydrocarbons become more reactive with increasing carbon number, lowering the decomposition temperature. The accelerated carbon formation might be attributed to weaker C–H bonding levels of 414 kJ/mol and 402.2 kJ/mol for C_2H_6 and C_3H_8, respectively, as compared to the bonding level of CH_4 of 440 kJ/mol [28].

Fig. 4 shows SEM images of carbon particles produced from the three kinds of hydrocarbons at different temperatures; Fig. 4(a1)–(a3) show carbon particles obtained from CH_4 decomposition at 700–900 °C, whereas Fig. 4(b1)–(b3) denote the case of C_2H_6 at 600–800 °C and Fig. 4(c1)–(c3) denote the case of C_3H_8 at 500–700 °C. As shown in Fig. 4(a1), CH_4 begins to decompose at 700 °C into a small quantity of carbon spheres (CS) with an average size of 72 ± 0.2 nm. In Fig. 4(a2) it can be seen that, following thermal decomposition at 800 °C, 285 ± 21 nm CS were well-dispersed with a higher population on the porous Ni anode surface. At 900 °C, slightly smaller CS of 162 ± 37 nm were produced, as shown in Fig. 4(a3), in a greater number compared to the sample obtained at 800 °C. As can be seen from Fig. 3, with the increased thermal decomposition of hydrocarbons, the CS were believed to form by homogeneous nucleation followed by coagulation or random condensation on the surface rather than by site-specific one-dimensional growth on the Ni surface [29].

Unlike the case of CH_4, C_2H_6 produced 1-dimensional carbon nanowires with diameters of 32 ± 0.8 nm and 28 ± 1.1 nm at 600 and 700 °C (see Fig. 4(b1) and (b2)), respectively. Interestingly, at 800 °C, carbon particles turn back to spherical particles (see Fig. 4(b3)). This morphology change is quite consistent with the observation of Kim et al. [30]; when carbon formation was highly

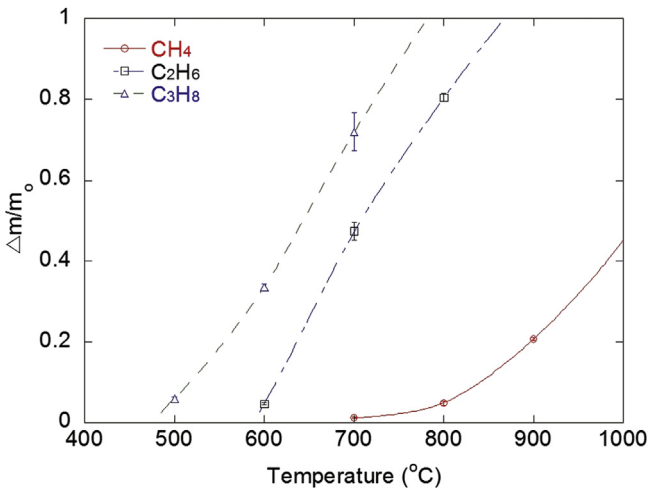

Fig. 3. Relative carbon mass formed inside a porous Ni anode through thermal decomposition of various hydrocarbons at different temperatures; the error bars represent standard deviations from the three repeated experiments.

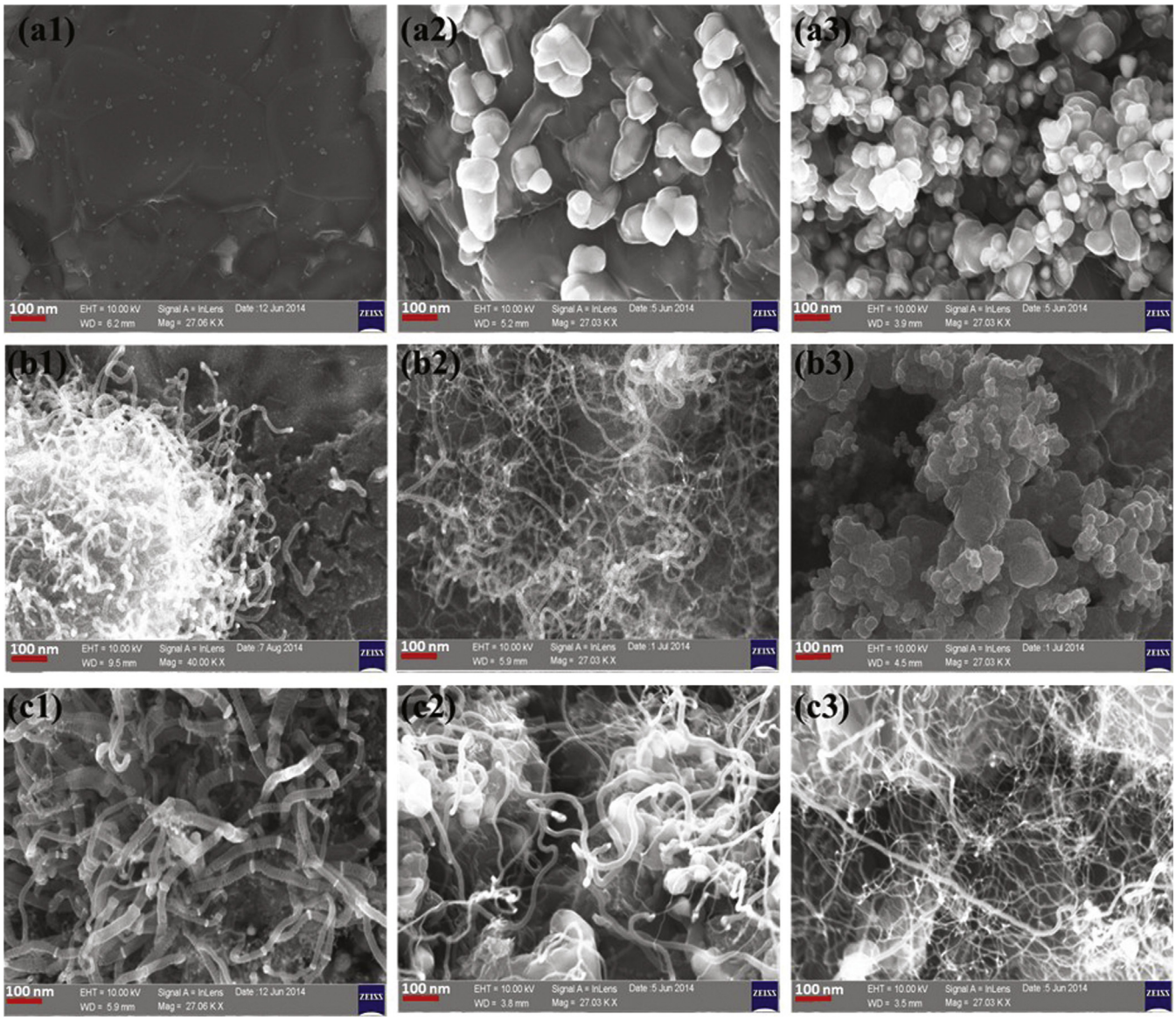

Fig. 4. SEM images of carbon samples produced from various hydrocarbons at different temperatures (stated in Fig. 3); (a1, a3) represents 700–900 °C for CH_4; (b1, b3) denotes 600–800 °C for C_2H_6; (c1, c3) does 500–700 °C for C_3H_8, respectively.

accelerated at high temperatures of 800–900 °C, the carbon particles tended to be amorphous or less crystallized and seemingly transformed into spherical shapes.

In a range of 500–700 °C of this study, only wire-like carbon particles were generated from C_3H_8; the amount of carbon increased with temperature as seen in Fig. 3. In Fig. 4(c1)–(c3), the wire diameter decreases significantly from 101 ± 0.5 nm, through 64 ± 2.2 nm to 24 ± 3.4 nm. As temperature increases in the range, the Ni surface could become more active to provide more sites allowing for 1-D growth of the wires. Provided that this temperature increase does not activate homogeneous nucleation [31,32], simultaneous formation of wires at elevated temperatures will make the wires thinner.

To determine the microstructure of the aforementioned wire-like carbons, HR-TEM was performed for the samples of C_2H_6 at 700 °C and C_3H_8 at 600 °C; the results are given in Fig. 5. Fig. 5(a1) shows that the 1-D nanowires shown in Fig. 4(b2) are indeed multi-walled carbon nanotubes (CNT) with outer diameter of ~30 nm. In Fig. 5(a2), the CNT wall was magnified 50 times and lattice fringe is in parallel with the wire axis. The lattice spacing was measured to be 0.344 nm, which is in good agreement with the lattice spacing of CNT reported by Ke et al. [33]. Fig. 5(b1) and 5(b2) show the morphology of wire-like carbons created from the condition shown in Fig. 4(c2). Fig. 5(b1) shows that the carbon wires appear to be covered with a layer as thick as 20–35 nm, which reminds of a kind of thicker carbon nanotubes. It should be noted, however, that seemingly solid-filled carbon wires coexisted even with a larger population than the hollow carbon wires. For reference, TEM image of the solid-filled carbon wires is shown in Fig. S1 of Supplementary data. How can we name the particles in Fig. 5(b1) and Fig. S1; carbon nanofibers or still nanotubes?

Many articles describe the difference between the carbon nanofibers (CNF) and carbon nanotubes (CNT) though they often look similar: 1) the diameter of CNT ranges from 10 to 30 nm while the CNF comes with diameters of 70–120 nm [34], 2) In CNT, graphene layers are wrapped as hollow cylinders whereas in CNF the graphene layers can be arranged as stacked cones, cups or plates often with an angle to the fiber axis [35], 3) CNF is considerably less

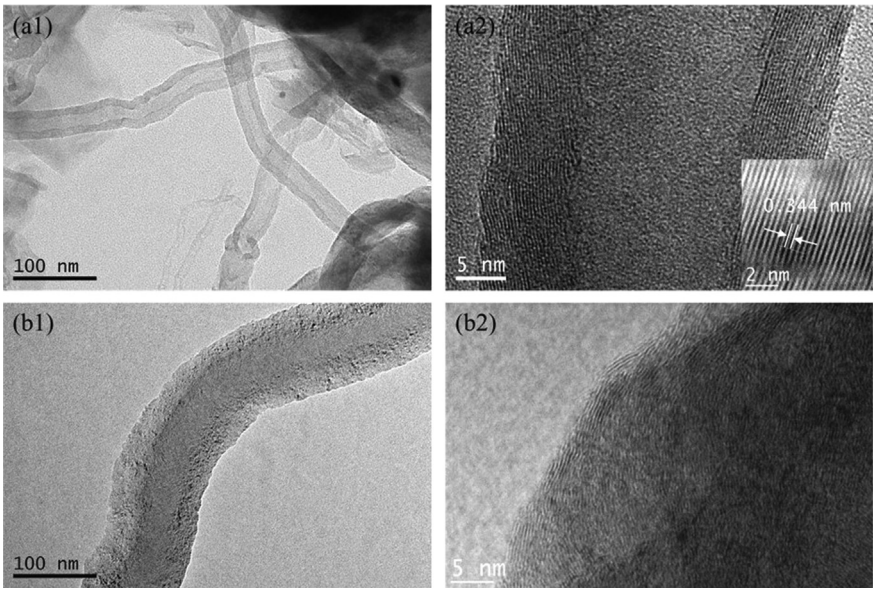

Fig. 5. HR-TEM images of (a1) CNT and (b1) CNF produced from C_2H_6 and C_3H_8; (a2) and (b2) are 50 times magnified from the images of (a1) and (b1), respectively.

crystallized than CNT [36]. Considering the size issue, the particles in Fig. 5(a1) are closer to the CNT whereas Fig. 5(b1) shows more likely the CNF. As for the second issue, there are several defected cracks (marked with arrows in the outer layer) that are perpendicular to the fiber axis in Fig. 5(b1). Similarly, inset of Fig. S1 denotes that carbon lattice fringe is aligned with a certain angle with respect to the fiber axis, which is another sign of CNF, in contrast to the parallel fringe in Fig. 5(a2). Overall, the particles in Fig. 5(b1) were conclusively named as CNF, being discriminated from the CNT in Fig. 5(a1).

The structural hardness or flexibility is related to the crystallinity of a solid; for example, amorphous solids can be more easily modified as they have greater flexibility compared to crystals [37]. Fig. 6 shows the results of Raman spectroscopy performed on the three carbon structures. Two Raman peaks were observed around 1350 cm^{-1} and 1583 cm^{-1} for all three samples. Both peaks are consistent with the well-known D and G band peaks at 1355 and 1596 cm^{-1} representing the sp^3- and sp^2-hybridized carbons, which have disordered and well-ordered lattice structures, respectively [38]. For CS generated from CH_4 decomposition (see Fig. 4(a2)), the G band peak is much higher than that of the D band. Since the ratio of the corresponding peak intensities (I_D/I_G), which represents the degree of disorderness in lattice structure, is the lowest at 0.46, the CS have relatively better crystallinity than others. On the other hand, the CNT from C_2H_6 (see Fig. 4(b2)) has the second highest I_D/I_G ratio of 0.86. For the CNF from C_3H_8 (see Fig. 4(c2)), the G band peak is inversely smaller than the D band peak, and the I_D/I_G ratio was the greatest at 1.35, suggesting that the CNF is most flexible.

Furthermore, XRD measurement was performed to test the crystallinity of the three samples. Fig. 6(b) shows that a distinct peak is observed for all samples at $2\theta = 26.2°$, corresponding to the (002) Bragg reflection of graphite. The CS shows the narrowest peak, representing the state of most crystallized lattice. The CNT with a few micrometers of length denotes a broader peak than the smaller CS, indicating that it is less crystallized. Most dramatic change is observed for the CNF. A very little and broad peak of the CNF implies that the CNF is the least crystallized or close to amorphous. These results are all consistent with those from Raman spectroscopy. Because electrochemical oxidation is affected by the crystallinity of solid fuels, the less crystallized CNT and CNF are expected to have better electrochemical kinetics compared to the case of CS [39].

To allow long-term use of C-containing Ni electrodes as DCFC anodes, the electrodes should stand against collapse for long periods of time at the operating temperature (700 °C) and include maximum allowed amounts of carbon. In case of CH_4, carbon particles of 1.2 wt% were produced within the porous electrode for 30 min at 700 °C (see Fig. 3). However, the electrode structure collapsed with swelling of the electrode when particles of 22.6 wt%

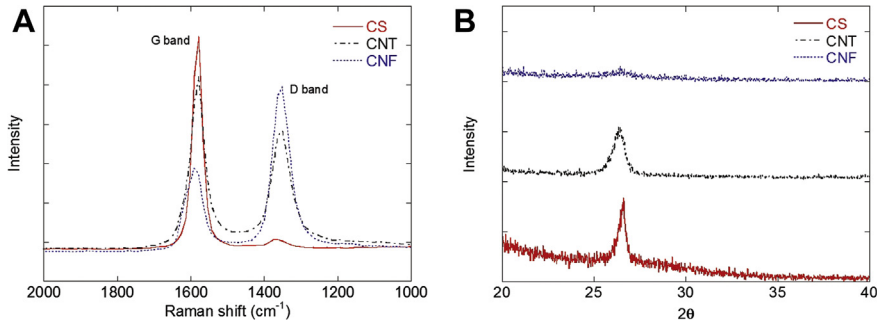

Fig. 6. (a) Raman spectra (a) and (b) X-ray diffractograms of three samples of CS, CNT and CNF.

were produced in a confined space during the same period of time at 900 °C. On the other hand, CS particles of 4.8 wt% were well-distributed on the anode surface at 800 °C, and did not cause any structural swelling of the anode. For this reason, 800 °C was selected as the decomposition temperature for fuel filling. Because the electrode structures in cases of C_2H_6 and C_3H_8 collapse at 800 °C and 700 °C, the lower temperatures of 700 °C and 600 °C were selected likewise, respectively. Of particular interest is to note that the electrodes did not collapse even though C_2H_6 and C_3H_8 produced 47 wt% of CNT at 700 °C and 33 wt% of CNF at 600 °C, much more than CH_4 at 900 °C for the same period of time (30 min). This implies that the CNF or even CNT are more flexible than the CS, which is consistent with the results of Raman spectroscopy and XRD results shown in Fig. 6. Finally, to compare the electrochemical characteristics of each fuel, the same amount (17.8 wt%) of carbon was generated in the same volume by adjusting the decomposition time to 4 h at 800 °C for CH_4, 18 min at 700 °C for C_2H_6, and 20 min at 600 °C for C_3H_8.

The three-electrode DCFC system in Fig. 2 was used to test the three kinds of porous Ni anode fueled with CS, CNT and CNF. Their electrochemical characteristics are compared for the different fuel types in Fig. 7. The CNT and CNF showed similar behavior in the potential-current density curve, while CS had a rapid potential decrease from OCV to 0.7 V, due to somewhat different characteristics: one possible explanation for the significant activation loss of the CS might be its having the highest degree of crystallinity, making it the least active. In this regard, it is not a surprise that the maximum power density of the CS is 240 mW/cm^2, and that the less ordered CNT and CNF fuels both had higher power density values of 380, 510 mW/cm^2, respectively.

Besides this, there might be another factor leading to the difference in the maximum power density; it might result from a difference in the morphology of the fuels inside the anode. Tubilla et al. [40] conducted electrochemical tests and EIS after depositing carbon/carbonate fuel on porous and non-porous GDC anodes at 800 °C, showing that porous anodes have a higher power density and lower charge transfer resistance (CTR) than those of non-porous anodes. They asserted that this was due to the increase in the contact area between the fuel and the electrodes. In the present study, the CTR values of the three kinds of fuels were measured by EIS at the OCV at 700 °C (see Fig. 8). Measurement at lower frequency was difficult because the data was a little noisy. The CTR of the CS is about 0.172 Ω cm^2, while the values of CNT and CNF are significantly lower than that of CS, at 0.1 and 0.095 Ω cm^2,

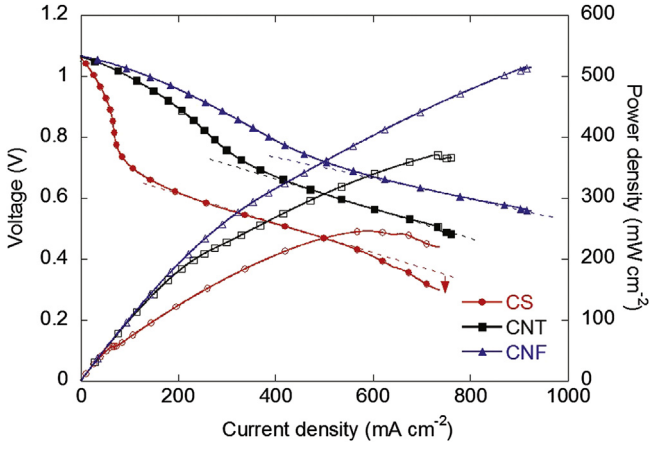

Fig. 7. Potential (V) and power density profiles against current density (I) for each carbon sample measured at 700 °C.

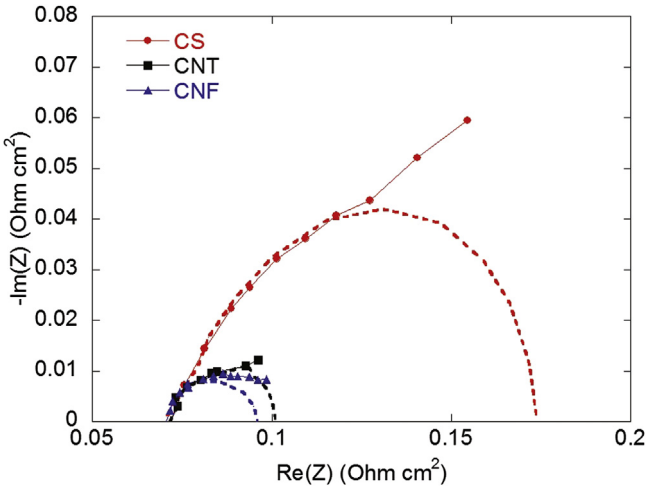

Fig. 8. Electrochemical impedance spectra of the three kinds of carbon samples operated at OCV condition.

respectively. This is probably due to the wire-like carbon's forming nets within the anode pores and acquiring a greater active area (particularly TPB) compared to case of CS.

Even though CNF and CNT have a similar value of CTR, there is a 36% difference in power density; this is presumed to be due to the influence of crystallinity-related reactivity. It might be plausible that less crystallized carbons are more reactive due to their elevated atomic mobility. Nevertheless, there is, to the best of our knowledge, no solid evidence of the crystallinity effect on the power density. One possible explanation can be made as follows. According to Rodriguez et al. [41], one of the most interesting features of CNF is the presence of large number of graphene edges exposed at the surface, which in turn constitutes specific sites readily available for chemical or physical interaction. CNTs, on the other hand, require complex processing methods that involve creation of defect sites along its side walls to make functionalized. Hence, we would postulate that the edges (possibly degrading the crystallinity) can serve as active sites at the surface of CNF, making the CNF more reactive than the CNT.

In Fig. 7, it is interesting to note that the V–I curves of CNT and CNF are almost linear in the entire high current area from 400 mA/cm^2 as guided with dotted lines, whereas the curve of CS loses its linearity from ~500 mA/cm^2 as indicated by an arrow. That means that the CS undergoes an additional resistance leading to further potential drop unlike others. Here, we would like to propose a morphology-related effect on the high-current cell performance, as follows. As depicted in Fig. 9(a1), CS establishes point contact with other spherical particles in a pore of the anode. As the CS can be an electron conductor, electrons generated on the surface of CS fuels can be transported to the current collector not only through regular pathways of the Ni networks (see dotted arrow lines) but also through the contacting particles themselves (see solid arrow lines). At high current densities, however, CS is gradually consumed at the surface, and particles might lose contact via separation. If this is the case, the loss of transport pathways makes electron transport less efficient and such an isolation of CS fuels lowers fuel utilization (see Fig. 9(a2)). On the other hand, CNT and CNF can transport electrons through wire-like structures instead of relying on point contact. Though carbon is consumed at the surface during the reaction, making the wires thinner, the electron transport pathway is still available so that the wires are able to maintain their power densities for longer periods than is possible for CS (see Fig. 9(b1, b2)).

In this regard, the long-term stability of the cell performance

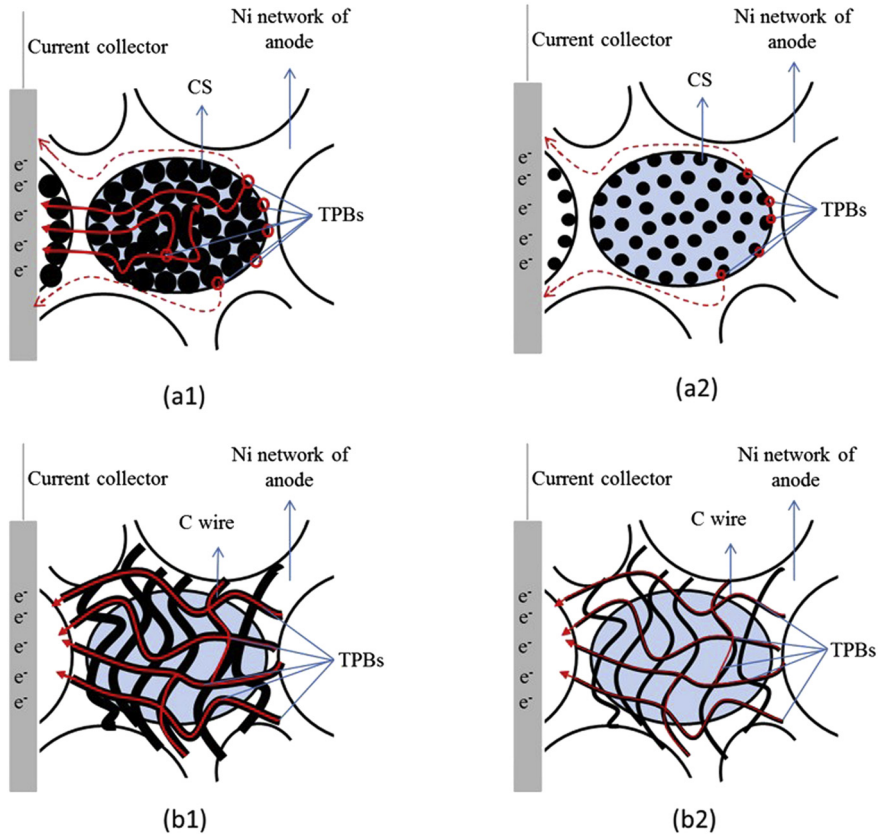

Fig. 9. Proposed mechanism for the morphology-related effect on the electrochemical reaction characteristics in terms of physical contact, triple phase boundary, and electron transport pathways.

was tested at a constant current density of 500 mA/cm^2 at 700 °C. Fig. 10 shows the potential vs time graph for the three types of carbon fuels. For CS, the potential decreased gradually from 0.7 V to 0.65 V for 3 min and then rapidly dropped down to 0 V within 12 min. As predicted in Fig. 9(a1, a2), the potential drop can be traced to isolation of passages of electron transport with increase in operation time. CNF and CNT showed slow decreases in potential from 0.8 to 0.7 V and 0.75 to 0.56 V, respectively, for the first 30 min. This was followed by a rapid potential drop resulting from complete consumption of fuel which would last up to 40 min. These results were consistent with the tendencies predicted in Fig. 9(b1, b2). Carbon-wire fuel cells can be considered capable of producing and transporting electrons with more efficient use of fuel than is possible when using spherical particles.

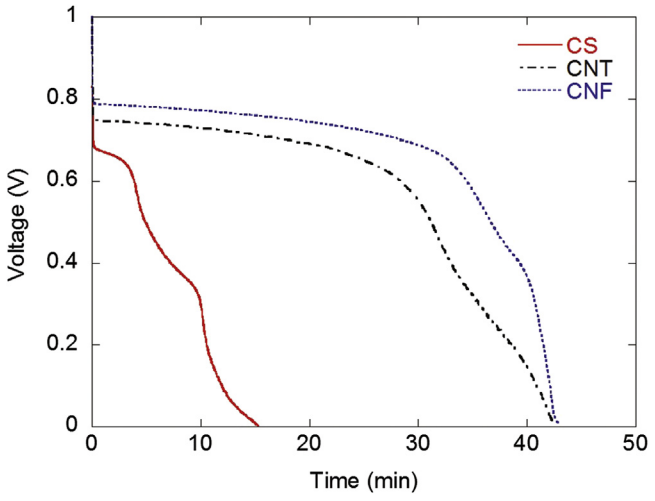

Fig. 10. Life time test results for the three different C-containing anodes at 700 °C.

4. Conclusions

In this study, we proposed a direct thermal decomposition of hydrocarbons in a porous Ni anode in an attempt to improve the physical contact between the electrode and carbon fuels. Three kinds of hydrocarbons with different carbon numbers (CH_4, C_2H_6, C_3H_8) were chosen and tested for the purpose at different temperatures. The resultant carbon particles had different morphologies: carbon spheres (CS), nanotubes (CNT), and nanofibers (CNF), depending on the carbon numbers. CNT and CNF were found to be less crystalline, more flexible compared to the CS obtained from CH_4. Temperature conditions (CH_4; 800 °C, C_2H_6; 700 °C, C_3H_8; 600 °C) for each hydrocarbon were set in consideration of anode durability. DCFC performance measured at 700 °C found that the 1-dimensional CNT and CNF were more active to produce 148% and 210% times higher power density than the CS. The difference in the performance was attributed to the differences in crystallinity and charge transfer resistance. A lifetime test found that CNT and CNF, capable of transporting electrons for longer time period, could produce the power stably for much longer periods, compared to CS which will lose their point contacts between the particles faster at high current density.

Acknowledgments

This work was supported by National Research Foundation of Korea (NRF) grants funded by the Korean Government (MEST) (No.

NRF-2010-0019543), and by the Human Resources Development Program (No. 20144010200780) of the Korea Institute of Energy Technology Evaluation and Planning (KETEP) grant funded by the Korea government Ministry of Trade, Industry and Energy. It was also supported by the Global Frontier R&D Program of the Center for Multiscale Energy Systems, funded by the National Research Foundation under the Ministry of Education, Science and Technology, Korea (No. 2012M3A6A7054863).

Appendix A. Supplementary data

Supplementary data related to this article can be found at http://dx.doi.org/10.1016/j.jpowsour.2015.06.079.

References

[1] S. Giddey, S.P.S. Badwal, A. Kulkarni, C. Munnings, Prog. Energy Combust. 38 (2012) 360–399.
[2] D. Cao, Y. Sun, G. Wang, J. Power Sources 167 (2007) 250.
[3] A. Elleuch, A. Boussetta, K. Halouani, J. Electroanal. Chem. 668 (2012) 99–106.
[4] D.G. Vutetakis, D.R. Skidmore, H.J. Byker, J. Electrochem. Soc. 34 (1987) 3027–3035.
[5] X. Li, Z. Zhu, R.D. Marco, J. Bradley, A. Dicks, Energy Fuels 23 (2009) 3721–3731.
[6] X. Li, Z.H. Zhu, R.D. Marco, A. Dicks, J. Bradley, S. Liu, G.Q. Lu, Ind. Eng. Chem. Res. 47 (2008) 9670–9677.
[7] X. Li, Z. Zhu, R.D. Marco, J. Bradley, A. Dicks, J. Power Sources 195 (2010) 4051–4058.
[8] J. Yu, Y. Zhao, Y. Li, J. Power Sources 270 (2014) 312–317.
[9] T.K. Lim, S.K. Kim, U.J. Yun, J.W. Lee, S.B. Lee, S.J. Park, R.H. Song, Int. J. Hydrogen Energy 39 (2014) 1–7.
[10] J. Jewulski, M. Skrzypkiewicz, M. Struzik, I.L. Radziejewska, Int. J. Hydrogen Energy 39 (2014) 21778–21785.
[11] J. Yu, B. Yu, Y. Li, Int. J. Hydrogen Energy 38 (2013) 16615–16622.
[12] K. Xu, C. Chen, H. Liu, Y. Tian, X. Li, H. Yao, Int. J. Hydrogen Energy 39 (2014) 17845–17851.
[13] Y. Nabae, K.D. Pointon, J.T.S. Irvine, J. Electrochem. Soc. 156 (2009) B716–B720.
[14] J. Liu, K. Ye, K. Cheng, G. Wang, J. Yin, D. Cao, Electrochim. Acta 135 (2014) 270–275.
[15] C. Li, Y. Shi, N. Cai, J. Power Sources 196 (2011) 4588–4593.
[16] S. Hasegawa, M. Ihara, J. Electrochem. Soc. 155 (2008) B58–B63.
[17] H. Saito, S. Hasegawa, M. Ihara, J. Electrochem. Soc. 155 (2008) B443–B447.
[18] M. Ihara, S. Hasegawa, J. Electrochem. Soc. 153 (2006) A1544–A1546.
[19] X. Li, Z. Zhu, R.D. Marco, J. Bradley, A. Dicks, Energy Fuels 23 (2009) 3721–3731.
[20] X. Xu, W. Zhou, F. Liang, Z. Zhu, Appl. Energy 108 (2013) 4022–4029.
[21] C. Li, E.K. Lee, Y.T. Kim, D. Lee, Int. J. Hydrogen Energy 39 (2014) 17314–17321.
[22] X. Xu, W. Zhou, F. Liang, Z. Zhu, Int. J. Hydrogen Energy 38 (2013) 5367–5374.
[23] A. Lanzini, P. Leone, C. Guerra, F. Smeacetto, N.P. Brandon, M. Santarelli, J. Chem. Eng. 220 (2013) 254–263.
[24] R. Bove, P. Lunghi, J. Power Sources 145 (2005) 588–593.
[25] D.A. Firmansyah, S.-G. Kim, K.-S. Lee, R. Zahaf, Y.H. Kim, D. Lee, Langmuir 28 (2012) 2890–2896.
[26] H. Lee, T.J. Kim, C. Li, I.D. Choi, Y.T. Kim, Z. Coker, T.-Y. Choi, D. Lee, Int. J. Hydrogen Energy 39 (2014) 14416–14420.
[27] P. Michael, R.A. Walker, Michael Brendan Scott Pomfret Doctor of Philosophy, 2007, pp. 174–175.
[28] N.Z. Muradov, Energy Fuels 12 (1998) 41–48.
[29] S.Y. Lu, C.H. Lin, J. Electrochem. Soc. 146 (1999) 4105–4110.
[30] S.H. Kim, M.R. Zachariah, J. Phys. Chem. B 110 (2006) 4555–4562.
[31] E.A. Solovyev, D.G. Kuvshinov, D.Y. Ermakov, G.G. Kuvshinov, Int. J. Hydrogen Energy 34 (2009) 1310–1323.
[32] B. Louis, G. Gulino, R. Vieira, J. Amadou, T. Dintzer, S. Galvagno, G. Centi, M.J. Ledoux, C. Pham-Huu, Catal. Today 102–103 (2005) 23–28.
[33] X. Ke, S. Bals, A.R. Negreira, T. Hantschel, H. Bender, G.V. Tendeloo, Ultramicroscopy 109 (2009) 1353–1359.
[34] H.A. Mohammed, S. Uttandaraman, Compos. Part A 42 (2011) 2126–2142.
[35] G. Tibbetts, M. Lake, K. Strong, B. Rice, Compos. Sci. Tech. 67 (2007) 1709.
[36] S. Vollebregt, R. Ishihara, F.D. Tichelaar, Y. Hou, C.I.M. Beenakker, Carbon 50 (2012) 3542–3554.
[37] D.A. Firmansyah, K. Sullivan, K.S. Lee, Y.H. Kim, R. Zahaf, M.R. Zachariah, D. Lee, J. Phys. Chem. C 116 (2012) 404–411.
[38] I.D. Choi, H. Lee, Y.B. Shim, D. Lee, Langmuir 26 (13) (2010) 11212–11216.
[39] M. Dudek, P. Tomczyk, R. Socha, M. Skrzypkiewicz, J. Jewulski, J. Electrochem. Soc. 8 (2013) 3229–3253.
[40] B.C. Tubilla, C. Xu, J.W. Zondlo, K. sabolsky, E.M. Sabolsky, J. Power Sources 145 (2005) 588–593.
[41] N.M. Rodriguez, A. Chambers, R.T.K. Baker, Langmuir 11 (1995) 3862.